OPEN ACCESS

University of Dundee

Bifurcations and chaotic dynamics in a tumour-immune-virus system

Eftimie, Raluca; Macnamara, C. K.; Dushoff, Jonathan; Bramson, J. L.; Earn, D. J. D.

Link to publication in Discovery Research Portal

Download date: 17. Feb. 2017

Bifurcations and chaotic dynamics in a tumour-immune-virus system

Raluca Eftimie[1] *, Cicely K. Macnamara[2], Jonathan Dushoff[3,4], Jonathan L. Bramson[4,5], David J.D. Earn[6]

[1] Division of Mathematics, University of Dundee, Dundee, United Kingdom, DD1 4HN

[2] School of Mathematics and Statistics, University of St. Andrews, St. Andrews, United Kingdom, KY16 9AJ

[3] Department of Biology, McMaster University, Hamilton, ON, L8S 4L8, Canada

[4] Michael G. DeGroote Institute for Infectious Disease Research, McMaster University, Hamilton, ON, Canada, L8N 4L8

[5] McMaster Immunology Research Centre, McMaster University, Hamilton, ON, Canada, L8S 4K1

[6] Department of Mathematics and Statistics, McMaster University, Hamilton, ON, Canada, L8S 4K1

Abstract. Despite mounting evidence that oncolytic viruses can be effective in treating cancer, understanding the details of the interactions between tumour cells, oncolytic viruses and immune cells that could lead to tumour control or tumour escape is still an open problem. Mathematical modelling of cancer oncolytic therapies has been used to investigate the biological mechanisms behind the observed temporal patterns of tumour growth. However, many models exhibit very complex dynamics, which renders them difficult to investigate. In this case, bifurcation diagrams could enable the visualisation of model dynamics by identifying (in the parameter space) the particular transition points between different behaviours. Here, we describe and investigate two simple mathematical models for oncolytic virus cancer therapy, with constant and immunity-dependent carrying capacity. While both models can exhibit complex dynamics, namely fixed points, periodic orbits and chaotic behaviours, only the model with immunity-dependent carrying capacity can exhibit them for biologically realistic situations, i.e., before the tumour grows too large and the experiment is terminated. Moreover, with the help of the bifurcation diagrams we uncover two unexpected behaviours in virus-tumour dynamics: (i) for short virus half-life, the tumour size seems to be too small to be detected, while for long virus half-life the tumour grows to larger sizes that can be detected; (ii) some model parameters have opposite effects on the transient and asymptotic dynamics of the tumour.

Keywords and phrases: cancer modelling, oncolytic viral therapy, global dynamics, chaos

Mathematics Subject Classification: 92C50, 65P20, 65P30

---

*Corresponding author. E-mail: `r.a.eftimie@dundee.ac.uk`

Raluca Eftimie, Cicely K. Macnamara, Jonathan Dushoff, Jonathan L. Bramson, David J.D. Earn
Bifurcation and Chaos in Tumour Dynamics

1. Introduction

Despite recent advances in molecular pathology, virology and genetics, permanent cancer elimination or even prolonged control of cancer are still elusive goals [8, 39, 48, 52, 53]. While there are experimental and clinical situations where cancers seem to be eliminated and patients cured [54], the majority of treatments only delay cancer recurrence [52].

Mathematical models can be used to understand and design new experiments, by formulating hypotheses regarding the potential biological mechanisms that could lead to delayed cancer relapse or to permanent elimination [8]. In fact, the last 10–20 years have seen an explosion in the number of deterministic mathematical models (both ODEs and PDEs) used to reproduce and further investigate different cancer therapies (see [2, 25] and references therein). Here, we will focus on ODE models, since they provide a simpler framework within which to explore the interactions among the different components of the tumour microenvironment [25]. In the context of these ODE models, we note that many simple models incorporate nonlinear terms that account for the spatial architecture of solid tumours [25]. Usually the first step (and sometimes the only step) in the analysis of such nonlinear mathematical models is to investigate the linear stability of steady states, with the purpose of identifying the mechanisms that ensure a stable tumour-free steady state. Biologically, this stability means that the tumour can be permanently eliminated, if it becomes sufficiently small. This approach is useful if the mathematical model has locally stable tumour-free steady states. However, many models of cancer immunotherapies display only unstable tumour-free steady states [13, 14, 34, 47].

The existence of unstable steady states can give rise to chaotic dynamics. For the past twenty years, chaotic behaviour has been proposed as a theoretical explanation for the unpredictability of cancer dynamics [18, 32, 38, 42, 43, 50, 55]. The presence of chaos, which causes the system to be unpredictable in the long term, also implies that the dynamics can be altered by small parameter variations [6]. Therefore, mathematical models for cancer growth that show chaotic behaviour might be useful for understanding the dynamics of the biological system and for proposing new biological mechanisms to control cancer [38].

In this article we focus on cancer immune and oncolytic virotherapies (i.e., therapies based on oncolytic viruses that replicate inside and destroy the cancer cells), which have expanded rapidly over the past decade and entered clinical trials [49]. The goal of this study is to show that the nonlinear interactions among the various components of the tumour microenvironment (e.g., immune cells, tumour cells, oncolytic virus particles) can induce surprising bifurcations, including bifurcations to chaotic dynamics. Understanding these transitions can help us better understand the type of models we use to describe the biological problem, and the appropriateness of these models. To our knowledge, chaotic dynamics has never previously been investigated in models for cancer-immune-virus interactions. Generally, these models focus on the analytical investigation of the steady states and their stability, and on the numerical investigation of the tumour and virus growth and spread patterns, with many studies also comparing the simulation results with available experimental data [3, 7, 22, 33, 51, 58, 61–64, 66]. By focusing on the chaotic aspects of models for tumour-immune-virus interactions, we aim to emphasise the complexity of the dynamics produced by these types of systems, which might explain the current unsuccessful oncolytic therapies. Moreover, we aim to show that some parameters that can be controlled experimentally can have opposite effects on the transient and asymptotic dynamics of the model (i.e., could lead to a decrease in tumour size during the transient dynamics and an increase in tumour size during the asymptotic dynamics).

To this end, we introduce a simple mathematical model that describes the interactions among cancer cells, immune cells and oncolytic viruses (i.e., viruses that selectively infect and replicate inside cancer cells). This model (which is a simplification of the model introduced in [27]) is based on a particular experimental protocol derived in [10] to investigate the combined anti-tumour effect of vaccination and oncolytic virotherapy. However, our model is sufficiently general to be applied to other combinations of cancer therapies. We show that this model can exhibit complex dynamics such as limit cycles and chaotic behaviour. Since these behaviours occur only after the tumour reaches its maximum size - as defined by the carrying capacity - we modify the model to introduce density-dependent carrying capacity (with

Raluca Eftimie, Cicely K. Macnamara, Jonathan Dushoff, Jonathan L. Bramson, David J.D. Earn
Bifurcation and Chaos in Tumour Dynamics

the magnitude of the immune response influencing the tumour carrying capacity). The new model can exhibit similarly complex dynamics but in slightly different parameter ranges. Since some of the model parameters are free (i.e., could not be identified from available data or from the literature), we also create bifurcation diagrams to visualise model dynamics when we vary these free parameters. With the help of these diagrams, we show that the chaotic dynamics exhibited by the two models would not necessarily be detected in experimental settings, since the amplitudes of chaotic oscillations are too low for detection. Moreover, we show that while some parameters have similar effects on the transient and asymptotic behaviour of the tumour (i.e., changes in the parameters lead to tumour reduction for both transient and asymptotic dynamics), other parameters can have opposite effects, by leading to a decrease in tumour size during transient dynamics, and an increase in tumour size for asymptotic dynamics.

We begin in Section 2 by describing the nonlinear ODE model for tumour-immune-virus dynamics. In Section 3, we discuss briefly the steady states and their linear stability, and then investigate numerically the model's transient and asymptotic dynamics indicating how chaos occurs for certain parameter ranges. In Section 4 we introduce a density-dependent carrying capacity for tumour growth, which depends on the level of tumour-infiltrating immune cells, and show that this new model can display experimentally-undetectable chaotic behaviour. In Section 5 we investigate the dynamics of the model as we vary the free parameters. We conclude in Section 6 with a discussion of the results.

2. Model description

The mathematical model we use to investigate the chaotic tumour-immune-virus dynamics follows an experimental protocol derived in [10]. The protocol (depicted graphically in Fig.1(a)) involves two viruses, a vaccine virus and an oncolytic virus, which carry the same tumour antigen and are administered consecutively into tumour-bearing mice. (The tumour cells – melanoma cells in [10] – are injected into mice a few days before treatment begins.) Generally, the first virus (the vaccine, Adenovirus in [10]) induces an immune response against the tumour antigens. The second virus (the oncolytic virus, Vesicular Stomatitis Virus in [10]), which is usually administered after the first immune response wanes, induces a much stronger anti-tumour immune response that could theoretically eliminate tumours. However, it was shown in [10] that the Vesicular Stomatitis Virus (VSV) eliminated tumours only in some mice.
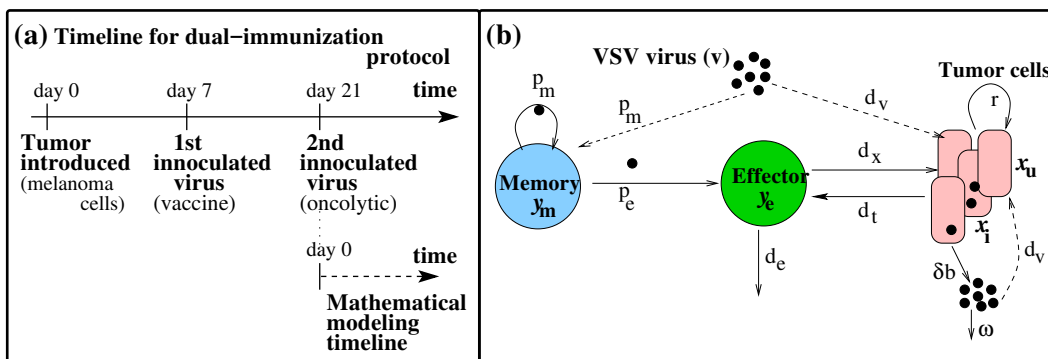
FIGURE 1. (a) Timeline for the dual-immunization protocol developed in [10], and for our mathematical model; (b) Graphical description of model (2.1). Once injected into the system, the virus particles will affect the tumour cells as well as the memory immune cells that become activated and differentiate into effector immune cells.

This immunisation protocol was first modelled and studied mathematically in [27], where the authors considered two compartments (lymphoid tissue – where the immune memory cells are located, and the peripheral tissue – where the tumour is located) to model the detailed interactions among tumour cells,

Raluca Eftimie, Cicely K. Macnamara, Jonathan Dushoff, Jonathan L. Bramson, David J.D. Earn
Bifurcation and Chaos in Tumour Dynamics

viruses, and immune cells. Despite the complexity of that model (described by seven equations), the authors were able to detect and investigate a multi-instability phenomena where all steady states were unstable. However, because of the large parameter space, the authors did not engage in a systematics search for chaos, and chaos was not detected for the parameter values investigated in [27].

Here, we introduce a simplified one-compartment model (see Figure 1(b)), which focuses only on the oncolytic virus, and considers a memory response induced by the injection of this virus following the vaccine virus. The state variables in this model are: the densities of infected (x_i) and uninfected (x_u) tumour cells, the densities of two types of immune cells: effector cells (y_e, cells that kill tumour cells) and memory cells (y_m, cells that proliferate in the presence of viral or tumour antigens), and the density of oncolytic virus particles (v). The model is described by the following equations:

$$\frac{dx_u(t)}{dt} = rx_u\Big(1 - \frac{x_u + x_i}{K}\Big) - d_v\frac{x_u v}{h_u + x_u} - d_x\frac{x_u y_e}{h_e + y_e}, \tag{2.1a}$$

$$\frac{dx_i(t)}{dt} = d_v\frac{x_u v}{h_u + x_u} - \delta x_i - d_x\frac{x_i y_e}{h_e + y_e}, \tag{2.1b}$$

$$\frac{dy_m(t)}{dt} = p_m\frac{v y_m}{h_v + v}\Big(1 - \frac{y_m}{M}\Big), \tag{2.1c}$$

$$\frac{dy_e(t)}{dt} = p_e\frac{v y_m}{h_v + v} - d_e y_e - d_t x_u y_e, \tag{2.1d}$$

$$\frac{dv(t)}{dt} = \delta b x_i - \omega v. \tag{2.1e}$$

Briefly, we assume that uninfected tumour cells grow logistically at intrinsic rate r (and have a carrying capacity K). This assumption approximates the natural deceleration in the growth as the size of the tumour increases [56]. The uninfected tumour cells can be infected with oncolytic viruses at rate d_v, and eliminated by the immune effector cells at rate d_x. The infected tumour cells have a mean lifetime of $1/\delta$ (determined by the timescale of virus replication within these cells), and are eliminated by the immune effector cells at rate d_x. In the presence of the oncolytic virus, memory cells proliferate logistically at rate p_m and with a carrying capacity M. (This logistic term models competition for space among memory cells [1].) At the time of proliferation, some memory cells differentiate into effector cells at rate p_e. Effector cells die at rate d_e, and are inactivated by tumour cells at rate d_t. Finally, the oncolytic virus v is produced at rate δ by the infected tumour cells (on average, each infected cell produces b virus particles), and has a mean lifetime of $1/\omega$. To keep the model as simple as possible, we assume that the death rate of memory cells is insignificant compared to their proliferation rate (i.e., equation (2.1c) does not include a decay term). This assumption is realistic, since memory cells are long-lived cells, capable of persisting in the host even in the absence of antigen. In contrast, most effector cells die during the contraction phase of the immune response [60]. A graphical description of this model is presented in Fig.1(b).

To account for the spatial structure of solid tumours, which may hinder the spread of viral particles or immune cells throughout the tumour [5,9], the terms describing the interactions among virus particles, immune cells, and tumour cells are chosen to be of Michaelis-Menten type [44]. These terms can also account for the heterogeneity of the tumour microenevironment, which might lead, for example, to reduced encounter rates between immune cells and infected tumour cells. We acknowledge here that the form of these interaction terms are just an example of possible interaction functions, other studies considering for example bi-linear interactions [62]. Therefore, the results presented here are particular to model (2.1).

3. Model analysis

3.1. Stability analysis

To understand the dynamics of model (2.1), we start by briefly discussing the linear stability of the steady states. Model (2.1) has four types of steady states:

Raluca Eftimie, Cicely K. Macnamara, Jonathan Dushoff, Jonathan L. Bramson, David J.D. Earn
Bifurcation and Chaos in Tumour Dynamics

(i) a tumour-free (TF) steady state: $(x_{\mathrm{u}}, x_{\mathrm{i}}, y_{\mathrm{m}}, y_{\mathrm{e}}, v) = (0, 0, y_{\mathrm{m}}^*, 0, 0)$, with $y_{\mathrm{m}}^* \in \mathbb{R}^+$;

(ii) a tumour-only (TO) steady state: $(x_{\mathrm{u}}, x_{\mathrm{i}}, y_{\mathrm{m}}, y_{\mathrm{e}}, v) = (x_{\mathrm{u}}^*, 0, y_{\mathrm{m}}^*, 0, 0)$, with $x_{\mathrm{u}}^* = K$ and $y_{\mathrm{m}}^* \in \mathbb{R}^+$;

(iii) a tumour with virus but no immune response (TV) steady state: $(x_{\mathrm{u}}, x_{\mathrm{i}}, y_{\mathrm{m}}, y_{\mathrm{e}}, v) = (x_{\mathrm{u}}^*, x_{\mathrm{i}}^*, 0, 0, v^*)$, with $x_{\mathrm{u}}^* = \frac{\omega h_{\mathrm{u}}}{d_{\mathrm{v}} b - \omega}$, $v^* = \frac{r(1 - x_{\mathrm{u}}^*/K)}{d_{\mathrm{v}}/(h_{\mathrm{u}} + x_{\mathrm{u}}^*) + r\omega/(\delta b K)}$, $x_{\mathrm{i}}^* = \frac{\omega v^*}{\delta b}$;

(iv) a steady state with all cell types and virus particles present (TVI): $(x_{\mathrm{u}}, x_{\mathrm{i}}, y_{\mathrm{m}}, y_{\mathrm{e}}, v) = (x_{\mathrm{u}}^*, x_{\mathrm{i}}^*, y_{\mathrm{m}}^*, y_{\mathrm{e}}^*, v^*)$, with $y_{\mathrm{m}}^* = M$.

We observe that the steady-state memory population y_{m}^* in the TF, TO and TVI states does not depend on model parameters associated with either the virus, tumour or effector cell populations ($y_{\mathrm{m}}^* = M$ or $y_{\mathrm{m}}^* = c$, with $c \in \mathbb{R}^+$ some constant). This makes sense biologically, since (a) there is a steady-state memory population following the first inoculation of the vaccine virus (see the vaccination protocol described in Figure 1(a)); (b) even if the tumour population becomes eliminated, the memory population continues to persist; (c) the memory population is long-lasting (in mice these cells can persist for years).

Of the four types of steady states, the TF and TV states are always locally unstable (see the discussion in Appendix B). In particular, the TF state is always a saddle point. The stability of the TO state is determined by the effective reproductive number (for the virus) associated with this state:

$$\mathcal{R}_{\mathrm{e}} = \frac{d_{\mathrm{v}} b}{\omega} \frac{x_{\mathrm{u}}^*}{h_{\mathrm{u}} + x_{\mathrm{u}}^*}. \tag{3.1}$$

In particular, the TO state is stable when $\mathcal{R}_{\mathrm{e}} < 1$ and unstable when $\mathcal{R}_{\mathrm{e}} > 1$. For the parameter values used in this paper (and described in Table 2), $\mathcal{R}_{\mathrm{e}} = 1$ at $\omega \approx 2.59$, which corresponds to a virus mean half-life of about 6.4 hours. Throughout this study, we restrict our investigation to values of $\omega < 2.59$ (i.e, virus half-life greater than 6.4 hours) for which the TO state is always unstable since $R_{\mathrm{e}} > 1$. In regard to the fourth steady state TVI, for the parameter values considered in this article, there is only one type of TVI state, which is stable for $\omega \geq 1.32$/day and unstable for $\omega < 1.32$/day. The stability of the TF, TO and TV states can be established analytically, while the stability of the TVI state can be established numerically, as discussed in [27] and here in Appendix B.

3.2. Transient and asymptotic behaviour of the system

Next, we investigate both the transient ($t < 200 - 500$ days) and asymptotic ($t > 1000$ days) dynamics of model (2.1), as we vary parameter ω, which describes the elimination rate of virus particles. We focus on this particular parameter since it can be manipulated experimentally: either by blocking viral clearance by the reticulo-endothelial cells in the liver [11], or by prolonging the extracellular half-life of VSV particles (from 3.5-8 hrs to almost double these values) through genetical manipulation of the virus [31].

In Figure 2 we show the transient behaviour of the tumour cells (panel (a)), virus particles (panel (b)), memory cells (panel (c)) and effector cells (panel (d)), for $\omega = 1.38$, corresponding to a virus half-life of $t_{1/2} = \ln(2)/\omega \approx 12$hr. We remark that tumour re-growth triggers an increase in the virus particles that replicate inside tumour cells, and an increase in the effector cell population. The level of effector cells is not high enough to eliminate the tumour cells - it can only reduce their level. However, this reduction in tumour size occurs only after the tumour reached its carrying capacity on day 80, and thus it is irrelevant from a treatment point of view (since the mice would be sacrificed by then [46]). Note that changes in the initial data (see Table 1) might impact the transient dynamics of the system, by leading to a delay or a faster increase in tumour growth.

One disadvantage of the use of VSV for clinical applications is its fast inactivation and elimination [9,31]. Thus recent experimental studies focused on different methods to increase the half-life of the virus [17,31]. In Figure 3 we investigate the transient dynamics of the tumour cells (and the immune cells in the inset) as we decrease ω from 1.39 to 1.0, corresponding to an increase in virus half-life up to ≈ 16.6hr. Note that, for all ω values, the tumour can be reduced to very low densities but not eliminated completely. Moreover, the reduction in ω leads to a delay in tumour relapse (e.g., for up to 150 days for $\omega = 1.0$).

In regard to the asymptotic dynamics of system (2.1), we have seen in Figure 2(a) that the tumour can approach a fixed point (e.g., when $\omega = 1.38$). In Figure 4 we show two more types of asymptotic

Raluca Eftimie, Cicely K. Macnamara, Jonathan Dushoff, Jonathan L. Bramson, David J.D. Earn
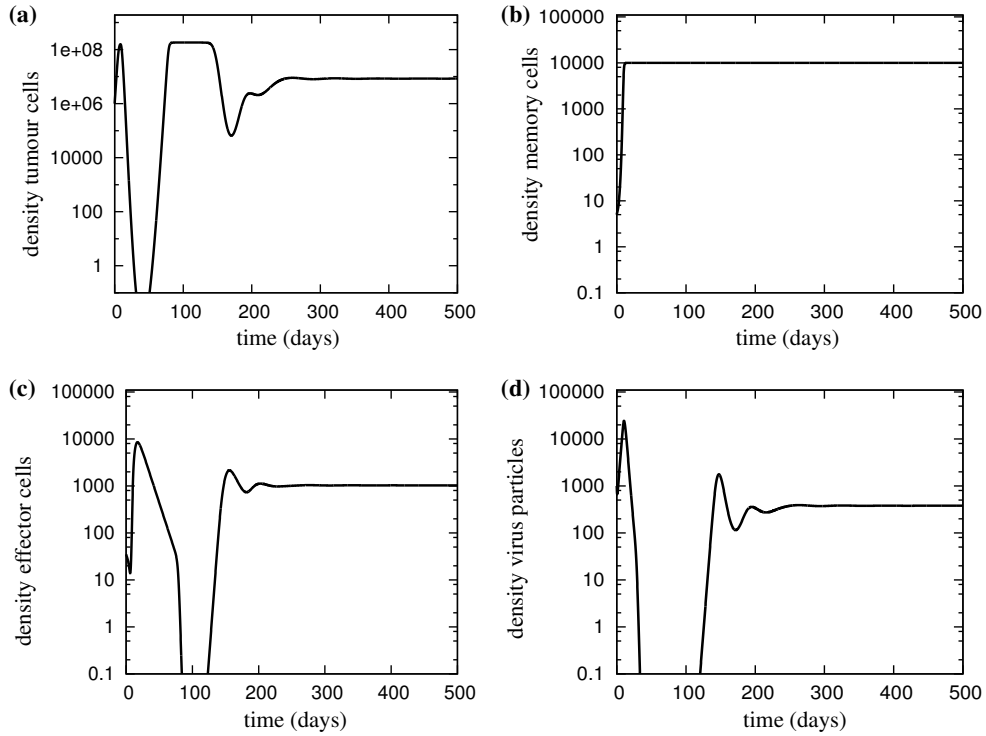Bifurcation and Chaos in Tumour Dynamics

FIGURE 2. An example of the transient dynamics of system (2.1) with the elimination rate of the oncolytic virus $\omega = 1.38$. We show (a) the tumour size, (b) the memory cell population, (c) the effector cell population, (d) the viral load. Here, the solution seems to approach the TVI state (with $y_m^* = M$ and $x_u^*, x_i^*, y_e^*, v^* > 0$). See Tables 1 and 2 for initial conditions and parameter values.

dynamics obtained as we decrease ω: (a),(d) periodic orbits; (b),(c) chaotic-type behaviours. In fact, as ω is decreased from $\omega = 1.38$/day to $\omega = 0.84$/day, the system undergoes a series of bifurcations from a steady-state (as in Figure 2(a), for $\omega = 1.38$/day) to periodic orbits (Figure 4(a), for $\omega = 1.29$/day), followed by inverse period-doubling bifurcations which then lead to chaotic fluctuations (Figures 4(b),(c), for $\omega = 1.26$/day or $\omega = 1.15$/day). As ω is decreased even further, the chaotic attractor collides with an unstable orbit, which causes the system to move to a periodic orbit (Figure 4(d); $\omega = 1.1$/day).

A clearer representation of this series of bifurcations is displayed in Figure 5. Panel (a) shows the local maximum values of $x_u(t)$, for simulations ran for $t \in [3000, 7000]$ days, and for $\omega \in [1.1, 1.29]$ - corresponding to the dynamics presented in Figure 4. We observe period doubling bifurcations for $\omega \in (1.267, 1.28)$, and a potential chaotic attractor for $\omega \in (1.19, 1.26)$ and again for $\omega \in (1.142, 1.167)$. In the inset, we show the first return map to a Poincaré section of the chaotic attractor built from the local maxima of tumour size, for the chaotic attractor at $\omega = 1.26$, constructed by plotting one tumour maximum against the previous maximum: $\max(x_u; n)$ vs. $\max(x_u; n-1)$; see [41]. In panel (b) we use the algorithm in [65] to calculate the largest Lyapunov exponent (LE) for each $\omega \in [1.1, 1.29]$, and confirm the existence of two regions of chaotic-like dynamics. We choose to plot the LE as it emphasises the parameter regions where we have chaos. To understand what happens in these two chaotic regions, we graph in panels (c), (d) and (e) the solution x_u for ω near 1.145 (panel (c)), ω near 1.2476 (panel (d)) and ω near 1.27 (panel (e)), where we know that chaotic-like behaviour occurs. Thus, as we slightly increase ω above $\omega = 1.145$ in panel (c), we obtain sequences of limit cycles of increasing periods (e.g., a period-5 cycle for $\omega = 1.145$, a period-6 cycle for $\omega = 1.1461$, and a period-7 cycle for $\omega = 1.1462$). Note that these limit cycles, are interspersed with chaotic dynamics - not shown here. In panel (d) we observe that

Raluca Eftimie, Cicely K. Macnamara, Jonathan Dushoff, Jonathan L. Bramson, David J.D. Earn
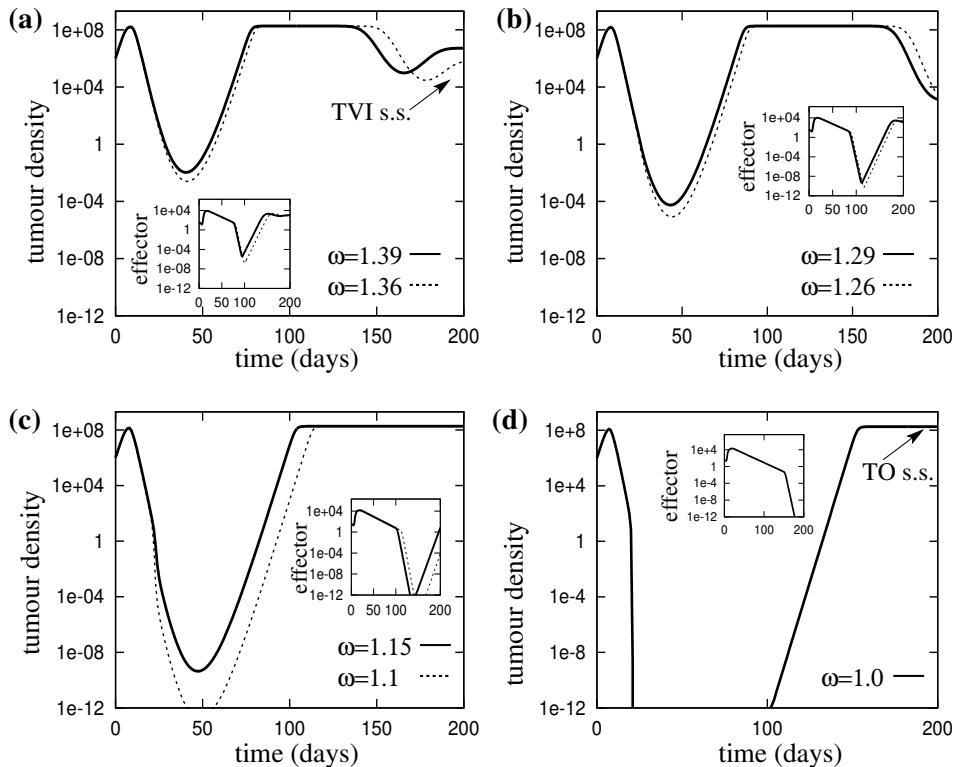Bifurcation and Chaos in Tumour Dynamics

FIGURE 3. The transient tumour dynamics of system (2.1) as the elimination rate of the oncolytic virus, ω, is decreased from $\omega = 1.39$/day to $\omega = 1.0$/day. The inset figures show the dynamics of the effector immune cells. The continuous and dashed lines show the dynamics of the tumour and immune cells for two different values of ω (in panel (b), the dynamics are quite similar, and the lines are hard to distinguish). See Tables 1 and 2 for initial conditions and parameter values.

for $\omega = 1.24766$, the trajectory visits the neighborhood of an unstable periodic orbit (during a so-called laminar phase) which is interrupted by a chaotic burst (at $t \approx 3550$), a behaviour which is typical from intermittencies, another route to chaos. Finally, in Figure 5(e) we show period-1 and a period-2 limit cycles, part of the period-doubling route to chaos observed in panel (a) for $\omega \approx 1.28$.

To summarise, we note that small changes in the decay rate ω may have little effect on the transient dynamics, but lead to different asymptotic dynamics. We need to emphasise that these conclusions depend on the initial conditions used for simulations (and described in Table 1). Also, the chaotic behaviour displayed by this ODE model is the results of various pathways to chaos: (i) the period-doubling route for $\omega \in (1.19, 1.27)$; (ii) the route to chaos via intermittency observed, for example, for $\omega \approx 1.24766$.

4. Immunity-dependent carrying capacity

The complex dynamics discussed in the previous section occurs after the tumour visits the neighbourhood of the TO steady state (i.e., the tumour carrying capacity), and thus is irrelevant from a treatment point of view (since in an experimental setting the mice would be euthanised when tumour becomes very large [46]). Next, we investigate the occurrence of chaotic dynamics when the tumour does not grow to such a large size.

The presence of immune cells inside the tumour micro-environment has been associated with good cancer prognosis [24, 29]. In particular, the presence of tumour-infiltrating immune cells has been associ-

Raluca Eftimie, Cicely K. Macnamara, Jonathan Dushoff, Jonathan L. Bramson, David J.D. Earn
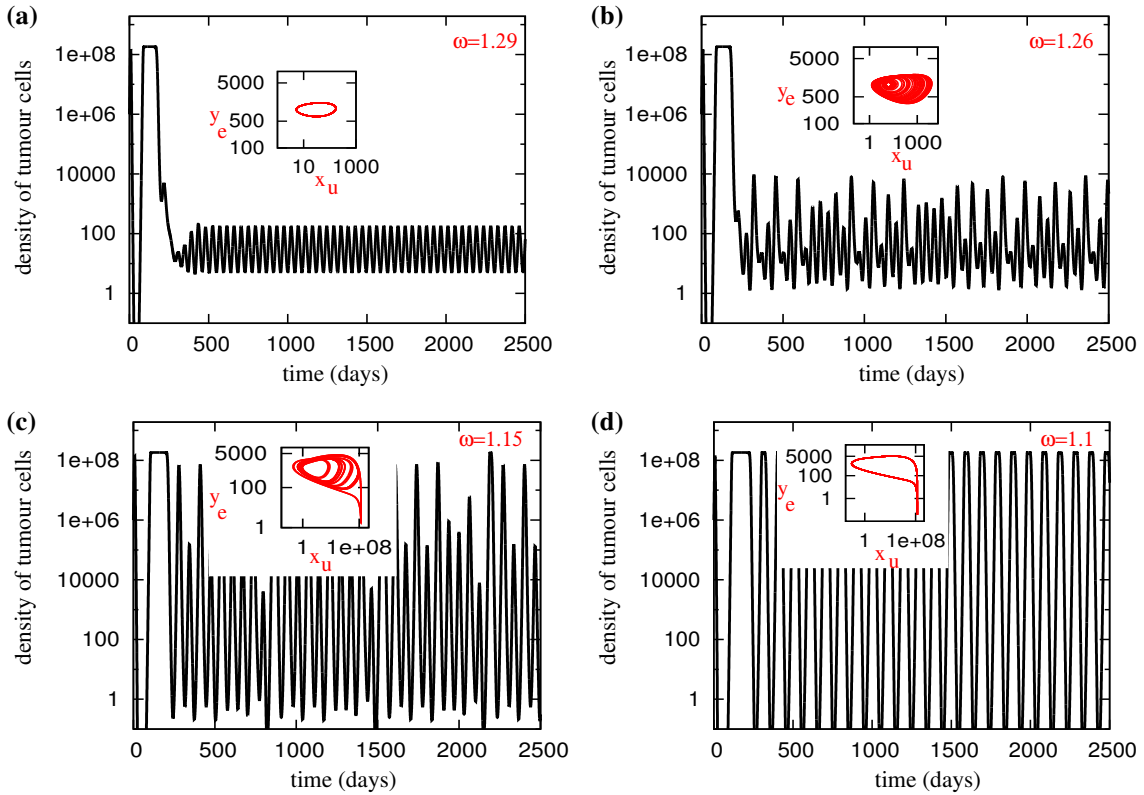Bifurcation and Chaos in Tumour Dynamics

FIGURE 4. Examples of asymptotic tumour dynamics of system (2.1) for: (a) $\omega = 1.29$, (b) $\omega = 1.26$, (c) $\omega = 1.15$, (d) $\omega = 1.1$. See Tables 1 and 2 for initial conditions and parameter values. The inset figures show the projection of model dynamics onto the $x_{\mathrm{u}} - y_{\mathrm{e}}$ plane, for time $t \in (500, 2500)$ days. For a more detailed depiction of the chaotic attractor obtained when $\omega = 1.26$, see Appendix C.

ated with a smaller tumour size and a lower tumour stage [24]. Therefore it is reasonable to assume that these immune cells could also impede the tumour to grow towards its carrying capacity (by secreting anti-angiogenic cytokines and promoting a tumour-hostile microenvironment [45]). Next we consider a slightly modified version of equation (2.1a), where the tumour carrying capacity is limited by the size of the immune response:

$$\frac{dx_{\mathrm{u}}(t)}{dt} = r x_{\mathrm{u}}\left(1 - \frac{x_{\mathrm{u}} + x_{\mathrm{i}}}{K - cy}\right) - d_{\mathrm{v}}\frac{x_{\mathrm{u}}v}{h_{\mathrm{u}} + x_{\mathrm{u}}} - d_{\mathrm{x}}\frac{x_{\mathrm{u}}y_{\mathrm{e}}}{h_{\mathrm{e}} + y_{\mathrm{e}}}. \tag{4.1}$$

Here, cy is a correction term to account for the fact that the tumour microenvironment will not support tumour growth towards its full carrying capacity. The variable y can be taken to be either or both immune populations, i.e., $y = y_m$, $y = y_e$ or $y = y_m + y_e$. The non-dimensional parameter c provides an indication of how "tumour hostile" the microenvironment is.

The density-dependent carrying capacity we consider here is different from the terms in [30, 37, 59], where the authors introduced separate equations for the evolution of tumour carrying capacity in response to pro-angiogenic signals produced by both immune and cancer cells, or in response to various pro-angiogenic and anti-angiogenic factors.

Next, we discuss not only the asymptotic dynamics of model (2.1)-(4.1) with density-dependent carrying capacity, but also its transient dynamics since: (i) this transient regime is important in experimental and clinical settings (which show variations in tumour growth patterns that are linked to variations in

Raluca Eftimie, Cicely K. Macnamara, Jonathan Dushoff, Jonathan L. Bramson, David J.D. Earn
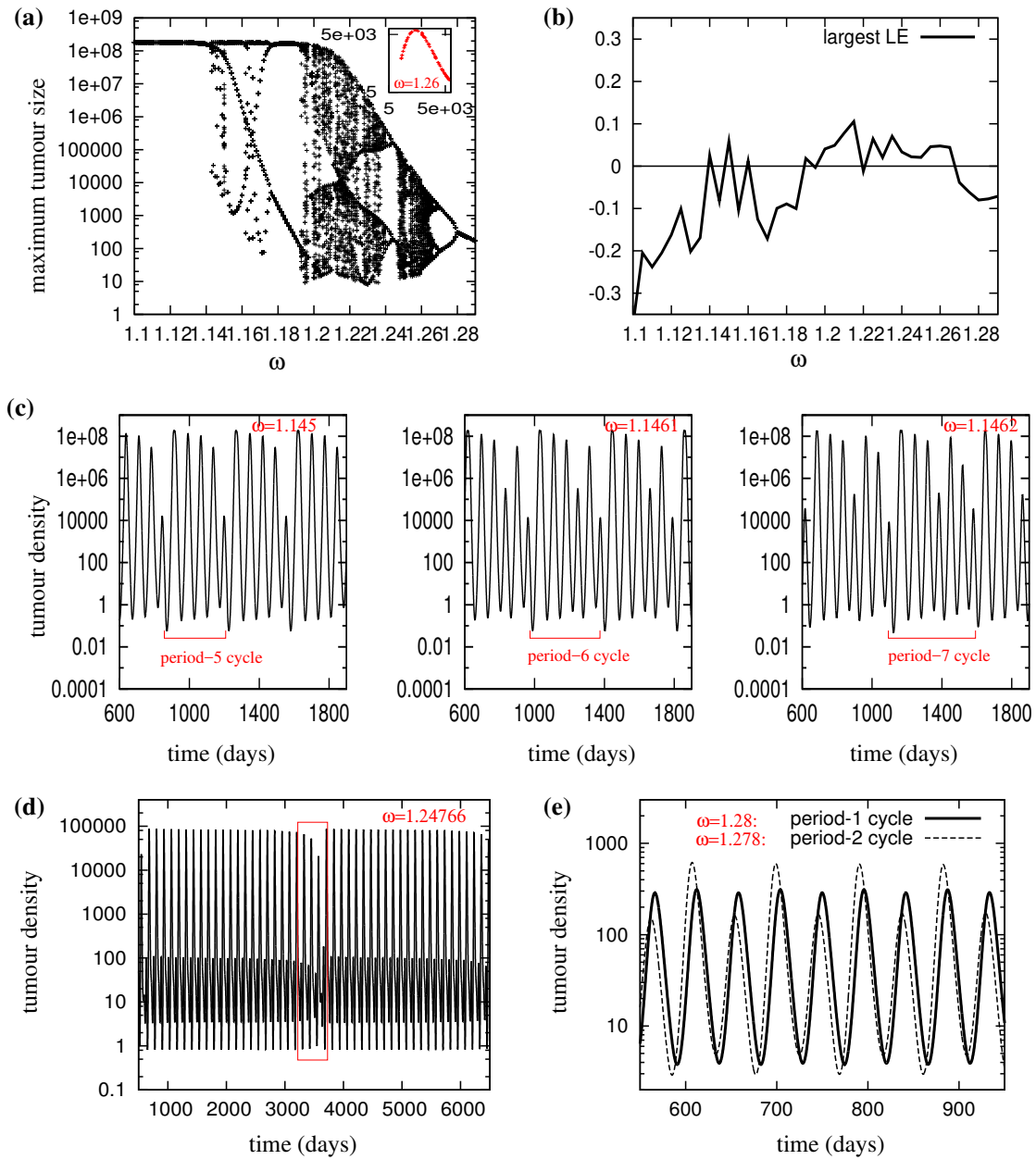Bifurcation and Chaos in Tumour Dynamics

FIGURE 5. (a) Maximum values of uninfected tumour cells x_{u}, for time $t \in (3000, 7000)$. For periodic solutions, this maximum is always the same. For chaotic solutions, the maximum values are very irregular. The inset shows the first-return map for the chaotic attractor at $\omega = 1.26$; (b) Largest Lyapunov exponent, for $\omega \in (1.1, 1.29)$; (c) Density x_{u} for $\omega = 1.145$, $\omega = 1.1461$ and $\omega = 1.1462$; (d) Density x_{u} for $\omega = 1.24766$; Note the irregular burst at $t \approx 3550$; (e) Density x_{u} for $\omega = 1.278$ and $\omega = 1.28$. See Tables 1 and 2 for initial conditions and parameter values.

the immune response - still difficult to understand due to the fact that initial conditions are not fully known/controlled in these settings [35]), and (ii) to emphasise the difference in the transient and asymptotic dynamics of the system.

Raluca Eftimie, Cicely K. Macnamara, Jonathan Dushoff, Jonathan L. Bramson, David J.D. Earn
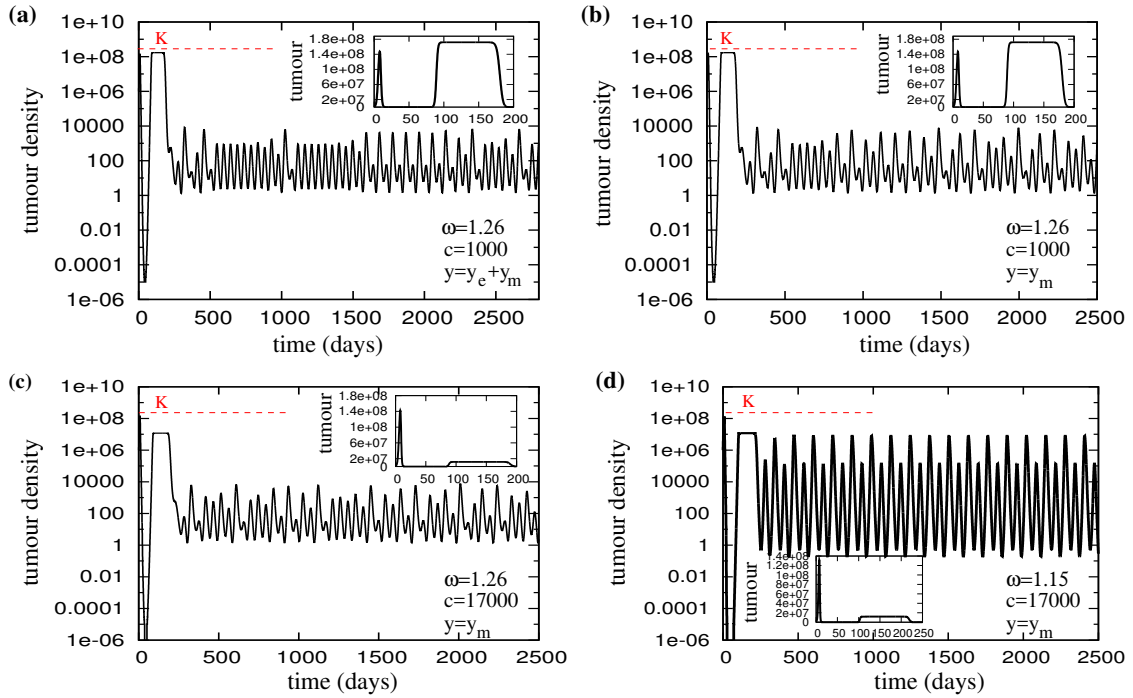Bifurcation and Chaos in Tumour Dynamics

FIGURE 6. Density of uninfected tumour cells x_u for different values of ω, c, and different choices of y variable. The dashed horizontal like shows the value of the carrying capacity K. The inset shows the transient tumour dynamics (i.e., $t < 200$). (a) $\omega = 1.26$, $c = 1000$ and $y = y_\mathrm{e} + y_\mathrm{m}$. (b) $\omega = 1.26$, $c = 1000$, $y = y_\mathrm{m}$. (c) $\omega = 1.26$, $c = 17000$, $y = y_\mathrm{m}$. (d) $\omega = 1.15$, $c = 17000$, $y = y_\mathrm{m}$. All other parameters are as in Table 2. Note that $y_m(t) + y_e(t) < K/c$ in all these simulations (not shown here).

Figure 6 shows the asymptotic and transient (in the inset) tumour dynamics for model (2.1b)-(2.1e) & (4.1), for particular values of ω, c and two choices of y-variable. In panels (a)-(b) we compare the choice of y variable ($y = y_m$ or $y = y_m + y_e$) on the tumour growth pattern, and notice that both $y = y_\mathrm{m} + y_\mathrm{e}$ and $y = y_\mathrm{m}$ lead to similar outcomes (and in all cases $\max(y) < K/c$; not shown here). This is the result of the memory response being much larger than the effector response, with memory cells also fast approaching their carrying capacity M. Because of this, in the following we assume that $y = y_\mathrm{m}$. In panels (b)-(c) we compare the choice of parameter c on the tumour growth patterns and observe that, as expected, larger c leads to lower maximum tumour sizes (see tumour size between days 100-200). The red dashed horizontal line shows tumour carrying capacity $K = 1.8 \times 10^8$, and for $c = 17000$ in panel (c), we observe that the maximum tumour size is below 10^7 cells/vol, which is the detection level of tumours (corresponding to a solid tumour diameter of 0.2 cm [28]). Finally, in panels (c)-(d) we compare the effect of ω on the tumour growth patterns when we fix c ($c = 17000$), and observe that chaotic dynamics can be lost when we decrease ω (e.g., to $\omega = 1.15$).

To have a better understanding of the effect of reducing the carrying capacity K on the dynamics of tumour growth, we show in Figure 7(a) a bifurcation diagram for the local maximum values of x_u versus $\omega \in [1.1, 1.29]$, as we fix $c = 17000$. We note that while there is no chaos for $\omega = 1.15$, chaos still persist for $\omega \in (1.22, 1.27)$. The inset shows the first-return map to a Poincaré section of the chaotic attractor at $\omega = 1.26$. We emphasise this persistence of deterministic chaos by showing in Figure 7(b) the largest Lyapunov exponent for system (2.1b)-(2.1e) & (4.1) versus $\omega \in (1.22, 1.27)$, when $c = 17000$. To investigate in more detail the effect of c on the persistence or absence of chaotic dynamics, in Figure 7(c),(d) we show bifurcation diagrams for the local maximum values of x_u versus $c \in [0, 17000]$, when

Raluca Eftimie, Cicely K. Macnamara, Jonathan Dushoff, Jonathan L. Bramson, David J.D. Earn
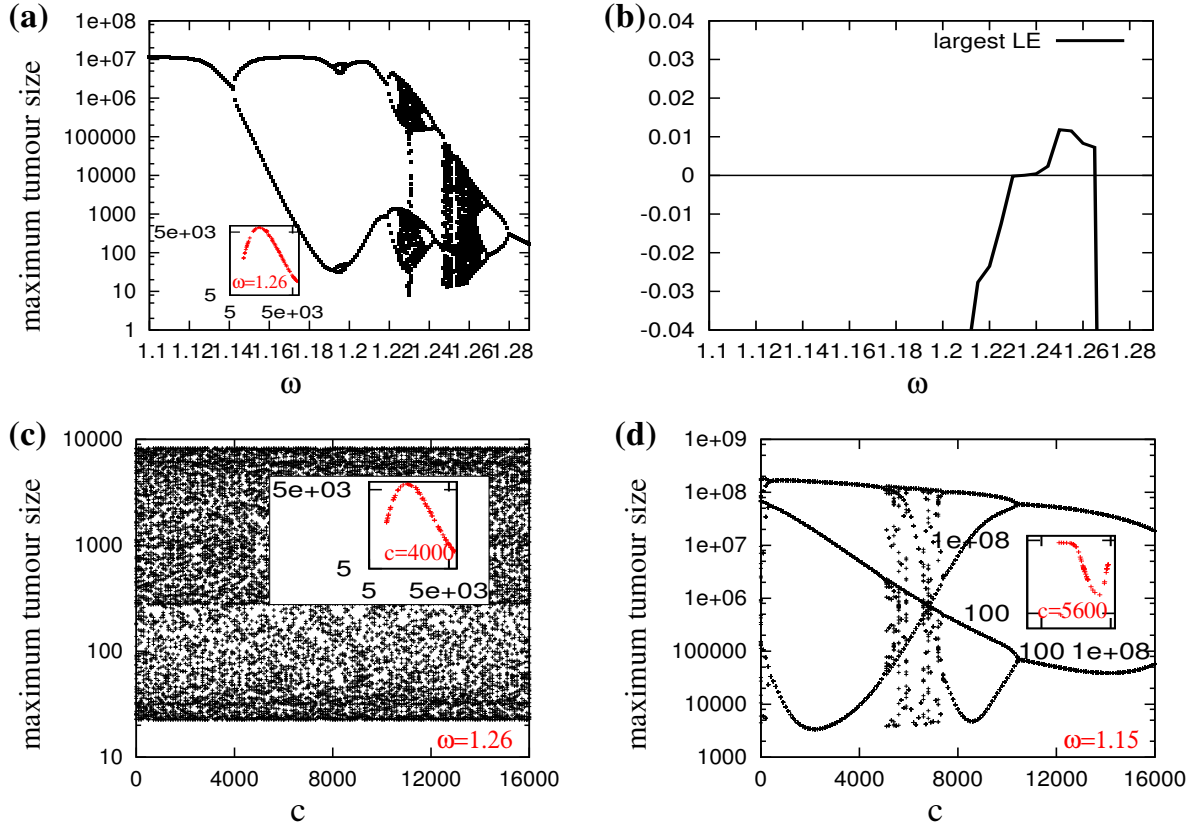Bifurcation and Chaos in Tumour Dynamics

FIGURE 7. Bifurcation diagrams corresponding to tumour dynamics described by equation (4.1). (a) Bifurcation of local maximum values of x_u (for $t \in [3000, 7000]$) versus $\omega \in [1.1, 1.29]$. Here $c = 17000$. The inset figure shows the first-return map for $\omega = 1.26$. (b) Largest Lyapunov exponent (LE) for $\omega \in [1.1, 1.29]$ and $c = 17000$. (c) Bifurcation of local maximum values of x_u (for a fixed $\omega = 1.26$) versus $c \in [0, 17000]$. The inset figure shows the first-return map for $c = 4000$. (d) Bifurcation of local maximum values of x_u (for a fixed $\omega = 1.15$) versus $c \in [0, 17000]$. The inset figure shows the first-return map for $c = 5600$.

$\omega = 1.26$ and $\omega = 1.15$, respectively. Note that for $\omega = 1.26$ chaos persists for any value of c (panel (c)), while for $\omega = 1.15$ chaos occurs for $c \in (5000, 7500)$ (panel (d)). The persistence of this chaotic behaviour for $\omega = 1.26$ is likely the result of asymptotic tumour sizes that are much lower than the tumour carrying capacity $K - cM$ (with M the carrying capacity of y_m cells), and thus variations in parameter c do not have any effect on these tumour sizes.

Finally, to investigate the parameter range where chaotic dynamics can or cannot be detected, we graph in Figure 8 the local maximum tumour sizes (for time $t \in (3000, 7000)$) as we vary parameter $\omega \in [1.1, 1.29]$ and parameter c: (a) $c = 0$, and (b) $c = 17000$. Recall that the detection level of tumours is at least 10^7 cells, which corresponds to a solid tumour with diameter of 0.2 cm [28]. We first observe that for $c = 17000$ the amplitude of the chaotic oscillations is always below 10^7 cells. However, for $c = 0$ the maximum amplitude can increase above 10^7 cells when $\omega < 1.23$ (corresponding to a virus half-life greater than 13.4hrs). For $\omega > 1.26$ (corresponding to a virus half-life less than 13.2hrs), the amplitude of the tumour chaotic oscillations is below 10^4, and thus it is unlikely that such oscillations can be observed experimentally (due to a lack of sufficiently accurate imaging techniques to measure temporal variations in tumour size). Overall, this is an unexpected behaviour since the persistence of VSV particles (i.e., low ω) would suggest that the tumour can be kept under control at smaller sizes.

Raluca Eftimie, Cicely K. Macnamara, Jonathan Dushoff, Jonathan L. Bramson, David J.D. Earn
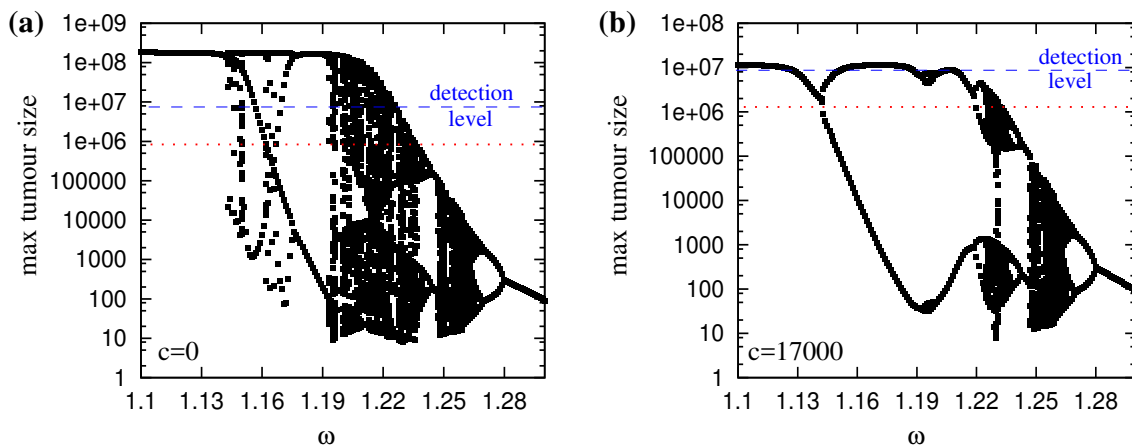Bifurcation and Chaos in Tumour Dynamics

FIGURE 8. Bifurcation dynamics for the maximum size of uninfected tumour cells x_u for $t \in (3000, 7000)$, as we vary the elimination rate of virus particles ω. The horizontal dotted red line shows the initial density of tumour cells, $x_u(0) = 10^6$. The horizontal dashed blue line shows tumour detection level $x_u \approx 10^7$. (a) Initial tumour growth model with $c = 0$; (b) Modified tumour growth model with $c = 17000$. See Tables 1 and 2 for initial conditions and parameter values.

5. Model sensitivity to "free" parameters

Since not all parameter values were known from the literature (see Table 2), in the following we investigate numerically the dynamics of model (2.1) when we vary the "free" parameters within the ranges shown in Table 2 (see column "Value"). We emphasise that we vary one parameter at a time, while keeping all other parameters fixed. Figure 9 shows bifurcation diagrams corresponding to asymptotic (i.e., $t \in (3000, 7000)$ days) changes in tumour size when we vary six estimated parameters: (a) d_v, (b) h_v, (c) h_u, (d) p_m, (e) p_e, (f) δ. The estimated values shown in Table 1 (and used throughout this study) are marked in these panels by a vertical dotted red line. The inset figures show the effect of these parameters on the transient tumour dynamics (i.e., on tumour size on day $t = 50$).

We notice in Figure 9(a) that large infection rates $d_v > 0.03$ do not have a significant impact on the asymptotic behaviour of the tumour (i.e., when $t \in (3000, 7000)$ days), but they do reduce the tumour size on day $t = 50$ (see the inset figure). Different effects in the transient and asymptotic behaviour of the tumour can also be observed when varying h_v, p_m and δ. The free parameters that show consistent effects on both the transient and asymptotic tumour behaviour are p_e (but only for $p_e > 0.2$) and h_u (but only for $h_u > 3$). The increase in p_e above $p_e = 0.2$ leads to a decrease in the transient and asymptotic tumour sizes. On the other hand, the increase in h_u above $h_u = 3$ leads to an increase in the transient and asymptotic tumour sizes. Finally, we note that the asymptotic dynamics of model (2.1) does not seem to be influenced by parameter p_m, the proliferation rate of memory cells; see Figure 9(d). This result is likely related to the fact that the memory cell population approaches quickly its carrying capacity, and thus the asymptotic dynamics of the tumour cannot be influenced anymore by variations in these memory cell numbers.

6. Summary and Discussion

In this article, we introduced a simple, nonlinear mathematical model that described the interactions among immune cells, cancer cells and viruses following oncolytic immunotherapy. Although this model was motivated by a specific protocol for cancer virotherapy [10], it could be used to describe other combinations of cancer immunotherapies, where an initial boost for the immune response is followed by a secondary boost caused by, for example, virus administration. We emphasise that this mathematical

Raluca Eftimie, Cicely K. Macnamara, Jonathan Dushoff, Jonathan L. Bramson, David J.D. Earn
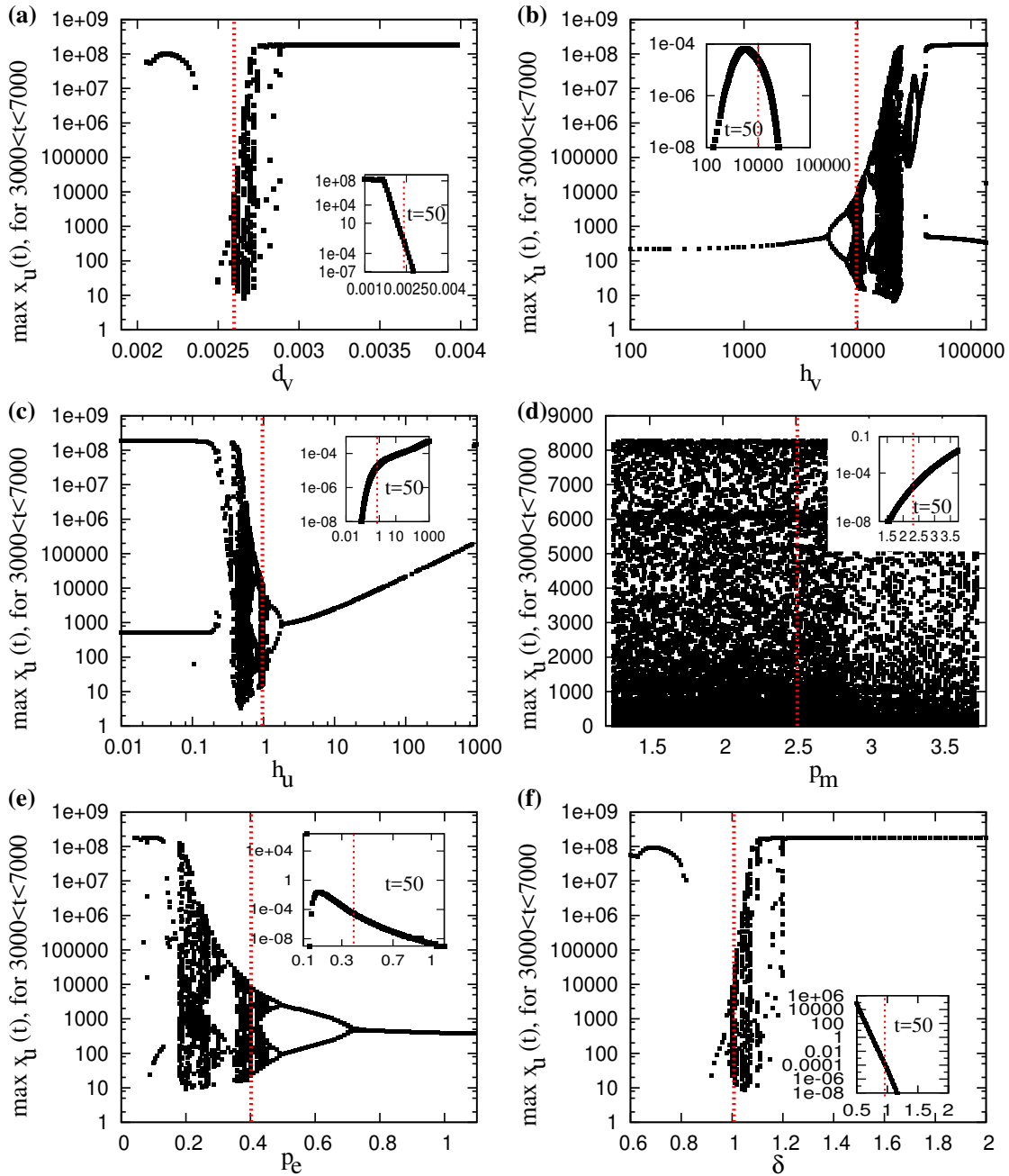Bifurcation and Chaos in Tumour Dynamics

FIGURE 9. Changes in the asymptotic and transient (in the inset) model dynamics, as we vary the free model parameters: (a) d_v, (b) h_v, (c) h_u, (d) p_m, (e) p_e, (f) δ. We choose here $\omega = 1.26$. The vertical red dotted line shows the estimated value (see also Table 2).

model is valid only for tumours that have not yet undergone angiogenesis. In addition, note that our discussion related to transient regime is very sensitive to initial conditions, and other initial conditions would have most likely led to different qualitative transient regimes.

Raluca Eftimie, Cicely K. Macnamara, Jonathan Dushoff, Jonathan L. Bramson, David J.D. Earn
Bifurcation and Chaos in Tumour Dynamics

We used this particular mathematical model to investigate the complex asymptotic dynamics of tumour-virus-immune interactions. First, we assumed a constant tumour carrying capacity and showed that the tumour will always approach this value (Figure 3). Moreover, we showed that after the tumour reaches its carrying capacity, the system could exhibit very complex dynamics which included fixed points, periodic orbits and chaotic behaviour (Figure 4). However, because these dynamics occurred after the tumour reached its carrying capacity, it was irrelevant from an experimental point of view (since mice are euthanised once the tumour becomes very large [46]).

To investigate whether complex dynamics can be observed also for smaller tumours, we modified the model to incorporate the assumption that the carrying capacity depended also on the density of tumour-infiltrated immune cells. The results showed that the tumour can grow to smaller or larger sizes, depending on how "tumour hostile" the microenvironment is (Figure 6). Moreover, we showed that the new model can also exhibit chaotic behaviour - although for slightly different parameter values (Figure 7).

We used bifurcation diagrams to investigate the parameter values for which chaotic dynamics can be detected in the original system (2.1), i.e., for which the asymptotic tumour size is above the threshold 10^7 cells (Figure 8). We showed that tumour detection requires a viral clearance rate $\omega < 1.23$ (equivalent to a virus half-life greater than 13.4hrs). This was completely unexpected since virus persistence is thought to lead to smaller tumours. For larger ω values (i.e., shorter virus half-life) chaotic dynamics could not be detected due to the very low amplitudes of oscillations. For these larger ω values the model could also exhibit periodic cycles, but their very low amplitudes made them undetectable. We note here that clinical oscillations in the immune response and tumour growth have been previously mentioned in the literature [16], although such reports are scarce. One possible explanation for the scarcity of these reports is the current lack of sufficiently accurate imaging techniques capable of measuring temporal variations in tumour size (to create relevant time series).

We also used bifurcation diagrams to test the sensitivity of our results to changes in the free parameters (i.e., parameters not identified from the literature; see Figure 9), and showed that some parameters have opposite effects on the transient (i.e., $t = 50$) and asymptotic (i.e., $t \in (3000, 7000)$) behaviour of the tumour size. For example, an increase in h_v above 10^4 leads to lower tumour size initially, but to higher tumour size in the long term. This suggests that anti-cancer treatments that work in the short term by reducing tumour size and delaying tumour relapse, might not work in the long term. This result may give insight into why to date oncolytic virotherapies have, on the whole, been unsuccessful [15]. More precisely, the (nonlinear) interactions between the multiple components of the tumour microenvironment - immune cells, cancer cells, virus particles - might explain tumour escape in the long term, via the complex global dynamics that they give rise to (in mathematical terms: multiple unstable steady states, limit cycles, chaotic dynamics, etc.). However, for a better understanding of the transient and long-term clinical and experimental observations, one needs to incorporate into the model more detailed dynamics of the signalling pathways that can be altered during cancer progression.

We would like now to discuss the unexpected behaviour in tumour-virus dynamics we mentioned previously, namely larger asymptotic tumour sizes (or larger amplitudes of chaotic oscillations) seem to correspond to longer virus persistence, i.e., smaller ω (see Figure 8). This is in complete contrast with the transient dynamics, where smaller ω leads to lower tumour sizes and delayed tumour re-growth (see Figure 3). It is unclear at this moment whether this unexpected observation regarding tumour-virus dynamics is an artefact of the mathematical model, or has been previously observed in the experiments. Many experimental approaches try to increase the circulating half-life of VSV, with the purpose of decreasing tumour size [57]. However, if the experimental approaches manage to keep the tumour under control at almost undetectable sizes, there will be no data comparing the asymptotic dynamics of these very low tumour sizes.

Throughout this study we focused mostly on the viral clearance rate ω (since it can be manipulated experimentally [11, 31, 57]). Due to the complexity of model equations, it is possible that changing other parameters could lead to different sorts of dynamical transitions. However, because of the very large parameter space, such an investigation was not the goal of this study. Rather, the goal was to emphasise the

Raluca Eftimie, Cicely K. Macnamara, Jonathan Dushoff, Jonathan L. Bramson, David J.D. Earn
Bifurcation and Chaos in Tumour Dynamics

necessity of investigating the asymptotic dynamics of the mathematical models (investigation performed here with the help of bifurcation diagrams), to obtain a better understanding of the non-linear effects of deterministic interactions among the various components of tumour microenvironments and to eventually generate new questions to be addressed experimentally.

Appendix A

The following two tables summarise the state variables (Table 1), and describe the parameter values used throughout this paper (Table 2). The majority of parameter values were obtained from the literature (see Table 2). There are a few "free" parameters (e.g., p_e, p_m, h_v, h_u, d_v) for which either we could not find specific values in the literature, or there were multiple contradictory values. In this case we estimated the values of these "free" parameters (the sole value in column *"Value"* in Table 2), and then we investigated the sensitivity of the model to these parameters for various parameter ranges (the intervals in column *"Value"* in Table 2).

State Variables	Meaning	Initial value
x_u	Density of uninfected cancer cells	10^6
x_i	Density of infected cancer cells	0
y_m	Immune memory cells	5
y_e	Immune effector cells	35
v	Density of oncolytic Vesicular Stomatitis Virus (VSV) particles	10^3

TABLE 1. State variables for model (2.1), and the initial values used in simulations.

The initial conditions in Table 1 are based on the experimental results in [10], where 10^6 B16-F10 tumour cells were injected into C57BL/6 mice. At the time of the injection, the number of CD8$^+$ T cells detected in blood (following previous priming with Ad+VSV vectors) was less than 250 cells/μl (which included both effector and memory cells; see Fig. S1 in [10]). Since the immune response following one viral vector is much lower than the immune response following two viral vectors (see Fig. S2 in [10]), for this theoretical study we chose $y_m(0) = 5$ and $y_e(0) = 35$. In [10], mice were injected VSV doses of at least 10^6 pfu. In our study, we investigated the effects of lower initial VSV loads ($v(0) = 10^3$). This lower value incorporates the assumption that only a small fraction of injected VSV particles reaches the tumour (see Fig. 4 in [10], where VSV brain titres were about $10^3 - 10^4$ pfu/g, in tumour-free and tumour-bearing murine brains).

In the following, we discuss some of the assumptions we made about model parameters:

– The B16 melanoma cells proliferate very fast in culture, with a doubling time of 14-19 hours [12]. Throughout this study, we consider a doubling time of about 18 hours, resulting in a proliferation rate $r = 0.927$ (see also [27]).
– The death rate δ of cells infected with VSV varies between studies: from $\delta = 0.69$/day in [51] to $\delta \in (0.665, 6.654)$/day in [7]. Throughout this study, we will choose $\delta = 1.0$/day, as in [27,33]. However, in Section 5, we investigate the model dynamics when $\delta \in (0.665, 6.654)$/day.

Raluca Eftimie, Cicely K. Macnamara, Jonathan Dushoff, Jonathan L. Bramson, David J.D. Earn
Bifurcation and Chaos in Tumour Dynamics

Parameter	Value	Units	Description & Reference
r	0.927	days^{-1}	proliferation rate for tumour cells [10, 12, 27]
K	$1/(5.5\times10^{-9})$	cells/vol	carrying capacity for the tumour cells [27]
d_v	0.0026 (0.002-0.004)	(cells/vol)(PFU/vol)$^{-1}$(days)$^{-1}$	infection rate of tumour cells with the oncolytic virus
d_x	2.6	days^{-1}	lysis rate of tumour cells (infected and uninfected) by the immune cells [36]
h_u	1 (10^{-2}-10^3)	cells/vol	half-saturation constant for the tumour cells infected with the oncolytic virus
h_e	2×10^3	cells/vol	half-saturation constant for the effector cells that support half the maximum killing rate [67]
h_v	10^4 (10^2-10^5)	PFU/vol	half-saturation constant of viral antigens that induce half the maximum proliferation rate of immune cells
δ	1.0 (0.665$-$6.654)	days^{-1}	rate at which the oncolytic virus kills the tumour cells [7, 27, 33]
p_m	2.5 (1.25-3.75)	days^{-1}	proliferation rate of memory cells following secondary encounter with tumour antigens carried by virus particles
M	10^4	(cells)/vol	carrying capacity for memory cells [4]
p_e	0.4 (10^{-2}-1.1)	days^{-1}	rate at which memory cells become effector cells following secondary encounter with tumour antigens carried by virus particles
d_e	0.1	days^{-1}	death rate of effector cells [4, 26]
d_t	5×10^{-9}	(cells)$^{-1}$(vol)(days)$^{-1}$	inactivation rate of immune effector cells by the tumor cells [27]
ω	$1.0 - 2.56$	days^{-1}	decay rate for the concentration of oncolytic virus (VSV) particles in the blood [9, 31]
b	1000	(PFU/vol)(cell)$^{-1}$(vol)	number of virus (VSV) particles released from an infected cell, capable of forming plaques [27]

TABLE 2. Parameters of model (2.1) and values used for numerical simulations. Some of the values were taken from the literature (as referenced). Throughout this article, we consider the density of cells: cell numbers per blood volume (vol). For mice, the blood volume is about 1.5-2.5ml. In the "Value" column, the numbers represent the values we used for the simulations in Sections 3-4, while the intervals represent the ranges used for the sensitivity analysis in Section 5.

– In [67], the authors showed that between 0.01-10% of CD8 T cells can become functional against melanoma. In regard to the effector functions of these cells, between 2-44% of them are producing IFN$-\gamma$ (i.e., an average of 2% of CD8 T cells in non-lymphoid tissue metastases, an average of 8% of cells in metastatic lymph nodes, and an average of 44% of cells obtained from peripheral blood mononuclear cells) [67]. In this study, we assume that an average of 20% of these effector cells contribute to the half-maximum immune response. Therefore, for a maximum density of effector cell $\approx 10^4$ (as for the memory cells from which they differentiate), we choose $h_\text{e} = 10^4 \times 20\% = 2 \times 10^3$ cells.

– The literature is very scarce in information on the level of virus particle necessary to trigger an infection. In the context of SIV infection in Rhesus macaques, [23] remarked that one viral copy of SIV RNA is enough for the spread of SIV infection. We could not find any information regarding the number of VSV particles necessary for the spread of VSV through tumour. Therefore, throughout this study we assume that the half-saturation constant for tumour cells infected with VSV is $h_\text{u} = 1$. Similar assumptions were made in [27]. However, in Section 5 we investigate model dynamics when $h_\text{u} \in (10^{-2} - 10^3)$.

Raluca Eftimie, Cicely K. Macnamara, Jonathan Dushoff, Jonathan L. Bramson, David J.D. Earn
Bifurcation and Chaos in Tumour Dynamics

– The intracellular half-life of nucleocapsids of VSV particles range from 5.3 hours to a maximum of 18 hours for certain virus mutants [21]. The extracellular half-life of VSV particles ranges between $3.5 - 8$ hours at $37°$C [31]. Throughout this work, we assume a virus half-life of $t^v_{1/2} \in (6.5, 16.5)$hours, which translates into a decay rate $\omega \in (1.0, 2.56)$/day. This range is more realistic than the value considered in [51] of $\omega = 0.1$ (for generalised logistic growth), corresponding to a VSV half life of ≈ 166 hours.
– The mathematical literature shows a wide range of immune cells inactivation rates by the tumour cells: from $d_t = 9.42 \times 10^{-12}$/(cells $\cdot$ day) in [19], to $d_t = 3.42 \times 10^{-10}$/(cells $\cdot$ day) in [20] and $d_t = 2.8 \times 10^{-9}$/(cells $\cdot$ day) in [40]. Here, we use the average value in [27]: $d_t = 5 \times 10^{-9}$/(cells $\cdot$ day).

Appendix B

Next, we discuss briefly the stability of the steady states of the model. To this end, we show first the Jacobian associated with system (2.1):

$$J = \begin{pmatrix} a_{11} & a_{12} & 0 & a_{14} & a_{15} \\ a_{21} & a_{22} & 0 & a_{24} & a_{25} \\ 0 & 0 & a_{33} & 0 & a_{35} \\ a_{41} & 0 & a_{43} & a_{44} & a_{45} \\ 0 & a_{52} & 0 & 0 & a_{55} \end{pmatrix},$$

with

$$a_{11} = r\left(1 - \frac{2x_u + x_i}{K}\right) - \frac{d_v v h_u}{(h_u + x_u)^2} - \frac{d_x y_e}{h_e + y_e}, \quad a_{12} = -\frac{r x_u}{K},$$

$$a_{14} = -\frac{d_x x_u h_e}{(h_e + y_e)^2}, \quad a_{15} = -\frac{d_v x_u}{h_u + x_u}, \quad a_{21} = \frac{d_v v h_u}{(h_u + x_u)^2},$$

$$a_{22} = -\delta - \frac{d_x y_e}{h_e + y_e}, \quad a_{24} = -\frac{d_x x_i h_e}{(h_e + y_e)^2}, \quad a_{25} = \frac{d_v x_u}{h_u + x_u},$$

$$a_{33} = \frac{p_m v}{h_v + v}\left(1 - \frac{2y_m}{M}\right), \quad a_{35} = \frac{p_m y_m h_v}{(h_v + v)^2}\left(1 - \frac{y_m}{M}\right), \quad a_{41} = -d_t y_e,$$

$$a_{43} = \frac{p_e v}{h_v + v}, \quad a_{44} = -d_e - d_t x_u, \quad a_{45} = \frac{p_e y_m h_v}{(h_v + v)^2}, \quad a_{52} = \delta b,$$

$$a_{55} = -\omega.$$

– The TF state is always unstable (a saddle point), since the the Jacobian matrix always has one positive eigenvalue: $\lambda_1 = r > 0$. (The other eigenvalues are $\lambda_2 = -\delta$, $\lambda_3 = 0$, $\lambda_4 = -d_e$, $\lambda_5 = -\omega$.)
– The eigenvalues corresponding to the TO state are $\lambda_1 = 0$, $\lambda_2 = -r$, $\lambda_3 = -d_e - d_t K$ and

$$\lambda_{4,5} = -0.5(\omega + \delta) \pm 0.5\sqrt{(\omega + \delta)^2 + 4\big(\delta b d_v K/(h_u + K) - \omega\delta\big)}.$$

Hence, the TO state can be stable or unstable, depending the value of $R_e = bd_v K/(\omega(h_u + K))$: if $R_e > 1$ then $\lambda_4 > 0$ and the steady state is unstable, while for $R_e < 1$ both $\lambda_{4,5} < 0$ and the steady state is stable.
– The TV steady state (which exists only when $d_v b > \omega$, equivalent to $R_e > 1$) has $y^*_m = 0$, which implies that $a_{35} = 0$. Hence, one of the eigenvalues of the Jacobian matrix calculated at the TV state is $\lambda_1 = p_m v^*/(h_v + v^*) > 0$ and thus this state is always unstable.
– The stability of the TVI state can be investigated only numerically (see the approach in [27]). It can be shown that this state is unstable for $\omega < 1.32$ (i.e., it is a saddle-focus with three real eigenvalues $\lambda_{1,2,3} < 0$, and two complex eigenvalues with $\text{Re}(\lambda_{4,5}) > 0$).

We can summarise these linear stability results in the following result:

Proposition .1. *For the parameters described in Table 2, model (2.1) has four different steady states with the following stability:*

Raluca Eftimie, Cicely K. Macnamara, Jonathan Dushoff, Jonathan L. Bramson, David J.D. Earn
Bifurcation and Chaos in Tumour Dynamics

1. *The tumour-free equilibrium (TF) is always unstable.*
2. *The tumour-only equilibrium (TO) is locally asymptotically stable if $R_e < 1$ and unstable if $R_e > 1$ (where R_e is given by (3.1)).*
3. *The tumour-with-virus (and no immune) equilibrium (TV) is always unstable.*
4. *The coexistence equilibrium (TVI), where all cells and viral particles are nonzero, is locally asymptotical stable if $\omega \geq 1.32$ and unstable if $\omega < 1.32$ (and all other parameters fixed as in Table 2).*

Appendix C

To obtain a better understanding of how the chaotic attractors are structured around the fixed points of system (2.1), we show in Figure 10 one such attractor in the $x_\mathrm{u} - y_\mathrm{e}$ plane, together with all fixed points corresponding to $\omega = 1.26$ (and all other parameters as in Table 2). For these particular parameters, the values of the fixed points of system (2.1) are as follows:

– TF: $(x_\mathrm{u}, x_\mathrm{i}, y_\mathrm{m}, y_\mathrm{e}, v) = (0, 0, 10^4, 0, 0)$;
– TO: $(x_\mathrm{u}, x_\mathrm{i}, y_\mathrm{m}, y_\mathrm{e}, v) = (1.81818181 \times 10^8, 0, 10^4, 0, 0)$;
– TV: $(x_\mathrm{u}, x_\mathrm{i}, y_\mathrm{m}, y_\mathrm{e}, v) = (0.94, 0.8716, 0, 0, 691.791)$;
– TVI: $(x_\mathrm{u}, x_\mathrm{i}, y_\mathrm{m}, y_\mathrm{e}, v) = (9.2693, 0.32, 10^4, 992.8991, 254.5433)$.

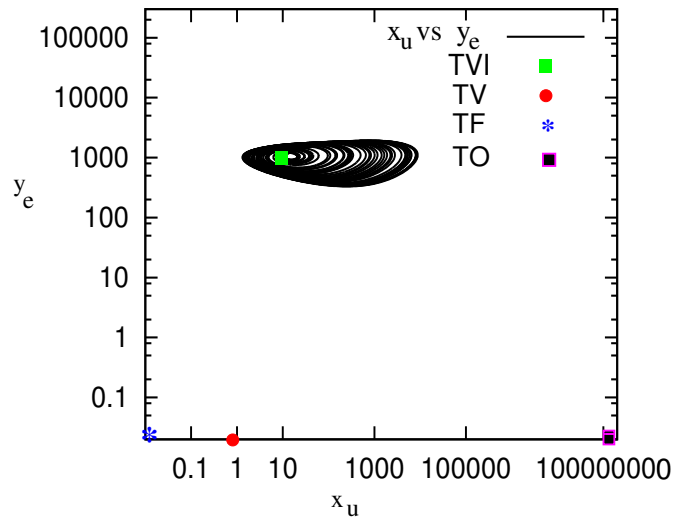We note that the chaotic attractor forms around the unstable TVI steady state.

FIGURE 10. Chaotic attractor (in the $x_\mathrm{u} - y_\mathrm{e}$ plane) exhibited by model (2.1), when $\omega = 1.26$ (and all other parameters as in Table 2). In addition, we show the fixed points TF, TO, TV and TVI (corresponding to these parameter values).

References

[1] R. Antia, S. Pilyugin, R. Ahmed. *Models of immune memory: on the role of cross-reactive stimulation, competition, and homeostasis in maintaining immune memory.* Proc. Natl. Acad. Sci. USA, 95 (1998), no. 25, 14926–14931.
[2] R.P. Araujo, D.L.S. McElwain. *A history of the study of solid tumor growth: the contribution of mathematical modeling.* Bull. Math. Biol., 66 (2004), 1039–1091.
[3] Z. Bajzer, T. Carr, K. Josić, S.J. Russell, D. Dingli. *Modeling of cancer virotherapy with recombinant measles viruses.* J. Theor. Biol., 252 (2008), 109–122.
[4] P.C.L. Beverley. *Primer: making sense of T-cell memory.* Nature Clinical Practice, 4 (2008), no. 1, 43–49.
[5] U. Blohm, D. Potthoff, A.J. van der Kogel, H. Pircher. *Solid tumors "melt" from the inside after successful CD8 T cell attack.* Eur. J. Immunol, 36 (2006), no. 2, 468–477.

[6] S. Boccaletti, C. Grebogi, Y.-C. Lai, H. Mancini, D. Maza. *The control of chaos: theory and applications.* Physics Reports, 329 (2000), 103–197.

[7] F. Le Boeuf, C. Batenchuk, M. Vähä-Koskela, S. Breton, D. Roy, C. Lemay, J. Cox, H. Abdelbary, T. Falls, G. Waghray, H. Atkins, D. Stojdl, J.S. Diallo, M. Kaern M, J.C. Bell. *Model-based rational design of an oncolytic virus with improved therapeutic potential.* Nat. Commun., 4 (2013), 1974.

[8] B.M. Boman, M.S. Wicha. *Cancer stem cells: a step toward the cure.* J. Clin. Oncol., 26 (2008), 2795–2799.

[9] C.J. Breitbach, J.M. Paterson, C.G. Lemay, T.J. Falls, A. McGuire, K.A. Parato, D.F. Stojdl, M. Daneshmand, K. Speth, D. Kirn, J.A. McCart, H. Atkins, J.C. Bell. *Targeted inflammation during oncolytic virus therapy severely compromises tumour blood flow.* Mol. Ther., 15 (2007), no. 9, 1686–1693.

[10] B.W. Bridle, K.B. Stephenson, J.E. Boudreau, S. Koshy, N. Kazdhan, E. Pullenayegum, J. Brunellière, J.L. Bramson, B.D. Lichty, Y. Wan. *Potentiating cancer immunotherapy using an oncolytic virus.* Mol. Ther., 18 (2010), no. 8, 1430–1439.

[11] K.T. Brunner, D. Hurez an R.T. McCluskey, B. Benacerraf. *Blood clearance rates of P_{32}-labeled Vesicular Stomatitis and Newcastle disease viruses by the reticuloendothelial system in mice.* J. Immunol., 85 (1960), 99–105.

[12] K.W. Brunson, G.L. Nicholson. *Experimental brain metastasis.* Brain metastasis (L. Weiss, H.A. Gilbert, J.B. Posner, eds.) Springer 1980 , 50–65.

[13] S. Bunimovich-Mendrazitsky, E. Shochat, L. Stone. *Mathematical model of BCG immunotherapy in superficial bladder cancer.* Bull. Math. Biol., 69 (2007), 1847–1870.

[14] H.M. Byrne, S.M. Cox, C.E. Kelly. *Macrophage-tumor interactions: In vivo dynamics.* Discrete and Continuous dynamical systems - Series B, 4 (2004), no. 1, 81–98.

[15] R.S. Coffin. *Oncolytic immunotherapy: an emerging new modality for the treatment of cancer.* Annals of Oncology (2016), 1–4.

[16] B.J. Coventry, M.L. Ashdown, M.A. Quinn, S.N. Markovic, S.L. Yatomi-Clarke, A.P. Robinson. *CRP identifies homeostatic immune oscillations in cancer patients: a potential treatment targeting tool?.* J. Translat. Med., 7 (2009), 102.

[17] M.A. Croyle, S.M. Callahan, A. Auricchio, G. Schumer, K.D. Linse, HJ.M. Wilson, L.J. Brunner, G.P. Kobinger. *PEGylation of a Vesicular Stomatitis Virus G pseudotyped lentivirus vector prevents inactivation in serum.* J. Virol., 78 (2004), 912–921.

[18] A. Dalgleish. *The relevance of non-linear mathematics (chaos theory) to the treatment of cancer, the role of the immune response and the potential for vaccines.* QJM, 92 (1999), no. 6, 347–359.

[19] L. de Pillis, A. Gallegos, A. Radunskaya. *A model of dendritic cell therapy for melanoma.* Frontiers in Oncology, 3 (2013), 56.

[20] L.G. de Pillis, A.E. Radunskaya, C.L. Wiseman. *A validated mathematical model of cell-mediated immune response to tumor growth.* Cancer. Res., 65 (2005), no. 17, 7950–7958.

[21] N.J. DePolo, J.J. Holland. *The intracellular half-lives of nonreplicanting nucleocapsids of di particles of wild type and mutant strains of vesicular stomatitis virus.* Virology, 151 (1986), no. 2, 371–378.

[22] D. Dingli, C. Offord, R. Myers, K.-W. Peng, T.W. Carr, K. Josic, S.J. Russell, Z. Bajzer. *Dynamics of multiple myeloma tumor therapy with a recombinant measles virus.* Cancer Gene Ther., 16 (2009), no. 12, 873–882.

[23] A. Durudas, H.-L. Chen, M.A. Gasper, V. Sundaravaradan, J.M. Milush, G. Silvestri, W. Johnson, L.D. Giavedoni, D.L. Sodora. *Differential innate immune responses to low or high dose of oral SIV challenge in Rhesus macaques.* Curr. HIV Res., 9 (2011), no. 5, 276–288.

[24] A.K. Eerola, Y. Soini, P. Pääkkö. *A high number of tumor-infiltrating lymphocytes are associated with a small tumour size, low tumour stage and a favourable prognosis in operated small cell lung carcinoma.* Clin. Cancer Res., 6 (2000), 1875–1881.

[25] R. Eftimie, J.L. Bramson, D.J.D. Earn. *Interactions between the immune system and cancer: a brief review of non-spatial mathematical models.* Bull. Math. Biol., 73 (2010), no. 1, 2–32.

[26] R. Eftimie, J.L. Bramson, D.J.D. Earn. *Modeling anti-tumor Th1 and Th2 immunity in the rejection of melanoma.* J. Theor. Biol., 265 (2010), no. 3, 467–480.

[27] R. Eftimie, J. Dushoff, B.W. Bridle, J.L. Bramson, D.J.D. Earn. *Multi-stability and multi-instability phenomena in a mathematical model of tumor-immune-virus interactions.* Bull. Math. Biol., 73 (2011), 2932–2961.

[28] S. Friberg, S. Mattson. *On the growth rates of human malignant tumours: implications for medical decision making.* J. Surgical Oncology, 65 (1997), 284–297.

[29] T.F. Gajewski, H. Schreiber, Y.-X. Fu. *Innate and adaptive immune cells in the timor microenvironment.* Nat. Immunol., 14 (2013), no. 10, 1014–1022.

[30] P. Hahnfeldt, D. Panigrahy, J. Folkman, L. Hlatky. *Tumor development under angiogenic signalling: a dynamical theory of tumor growth, treatment response, and post vascular dormancy.* Cancer Res., 59 (1999), 4770–4775.

[31] B.-Y. Hwang, D.V. Schaffer. *Engineering a serum-resistant and thermostable vesicular stomatitis virus G glycoprotein for pseudotyping retroviral and lentiviral vectors.* Gene Therapy, 20 (2013), 807–815.

[32] I.P. Janecka. *Cancer control through principles of systems science, complexity, and chaos theory: a model.* Int. J. Med. Sci., 4 (2007), 164–173.

[33] P.S. Kim, J.J. Crivelli, I.-K. Choi, C.-O. Yun, J.R. Wares. *Quantitative impact of immunomodulation versus oncolysis with cytokine-expressing virus therapeutics.* Mathematical Biosciences and Engineering, 12 (2015), no. 4, 841–858.

[34] D. Kirschner, J.C. Panetta. *Modeling immunotherapy of the tumor-immune interaction.* J. Math. Biol., 37 (1998), 235–252.

Raluca Eftimie, Cicely K. Macnamara, Jonathan Dushoff, Jonathan L. Bramson, David J.D. Earn
Bifurcation and Chaos in Tumour Dynamics

[35] K.M. Kokolus, M.L. Capitano, C.-T. Lee, J.W.-L. Eng, J.D. Waight, B.L. Hylander, S. Sexton C.-C. Hong, C.J. Gordon, S.I. Abrams, E.A. Repasky. *Baseline tumour growth and immune control in laboratory mice are significantly influenced by subthermoneutral housing temperature.* Proc. Natl. Acad. Sci. USA, 110 (2013), no. 50, 20176–20181.

[36] T.M. Kündig, M.F. Bachmann, S. Oehen, U.W. Hoffmann, J.J.L. Simard, C.P. Kalberer, H. Pircher, P.S. Ohashi, H. Hengartner, R.F. Zinkernagel. *On the role of antigen maintaining cytotoxic T-cell memory.* Proc. Natl. Acad. Sci. USA, 93 (1996), 9716–9723.

[37] U. Ledzewicz, H. Schättler. *Antiangiogenic therapy in cancer treatment as an optimal control problem.* SIAM. J. Control Optim., 46 (2007), 1052–1079.

[38] C. Letellier, F. Denis, L.A. Aguirre. *What can be learned from a chaotic cancer model?.* J. Theor. Biol., 322 (2013), 7–16.

[39] Q.-X. Li, Guohong Liu, F. Wong-Staal. *Oncolytic virotherapy as a personalized cancer vaccine.* Int. J. Cancer, 123 (2008), 493–499.

[40] A.G. Lópea, J.M. Seoane, M.A.F. Sanjuán. *A validated mathematical model of tumour growth including tumour-host interaction, cell-mediated immune response and chemotherapy.* Bull. Math. Biol., 76 (2014), 2884–2906.

[41] E.N. Lorenz. *Deterministic nonperiodic flow.* J. Atmospheric Sciences, 20 (1963), 130–141.

[42] M.C. Mackey, L. Glass. *Oscillations and chaos in physiological control systems.* Science, 197 (1977), 287–289.

[43] T. Mattfeldt. *Nonlinear deterministic analysis of tissue texture: a stereological study on mastopathic and mammary cancer tissue using chaos theory.* J. Microscopy, 185 (1997), no. 1, 47–66.

[44] J.D. Murray. *Mathematical Biology I. An Introduction.* Springer 2002.

[45] A. Naldini, F. Carraro. *Role of inflammatory mediators in angiogenesis.* Current Drug Targets - Inflammation & Allergy, 4 (2005), 3–8.

[46] N.I.H., O.A.C.U.. *Guidelines for endpoints in animal study proposals.* 1996 `http://oacu.od.nih.gov/ARAC/documents/ASP\_Endpoints.pdf`.

[47] M.R. Owen, J.A. Sherratt. *Modeling the macrophage invasion of tumors: effects on growth and composition.* Mathematical Medicine and Biology, 15 (1998), 165–185.

[48] K.A. Parato, D. Senger, P.A.J. Forsyth, J.C. Bell. *Recent progress in the battle between oncolytic viruses and tumors.* Nature Reviews Cancer, 5 (2005), 965–976.

[49] M.R. Patel, R.A. Kratzke. *Oncolytic virus therapy for cancer: the first wave of translational clinical trials.* Transl. Res., 161 (2013), no. 4, 355–364.

[50] T.D. Pham, K. Ichikawa. *Spatial chaos and complexity in the intracellular space of cancer and normal cells.* Theoretical Biology and Medical Modeling, 10 (2013), 62.

[51] D.M. Rommelfanger, C.P. Offord, J. Dev, Z. Bajzer, R.G. Ville, D. Dingli. *Dynamics of melanoma tumor therapy with vesicular stomatitis virus: explaining the variability in outcomes using mathematical modeling.* Gene Ther., 19 (2012), no. 5, 543–549.

[52] S.A. Rosenberg, J.C. Yang, N.P. Restifo. *Cancer immunotherapy: moving beyond current vaccines.* Nature Medicine, 10 (2004), 909–915.

[53] S.J. Russell, K.-W. Peng, J.C. Bell. *Oncolytic virotherapy.* Nat. Biotechnol., 30 (2012), no. 7, 658–670.

[54] D. Sargent, A. Sobrero, A. Grothey, M.J. O'Connell, M. Buyse, T. Andre, Y. Zheng, E. Green, R. Labianca, C. O'Callaghan, J.F. Seitz, G. Francini, D. Haller, G. Yothers, R. Goldberg, A. de Gramont. *Evidence for cure by adjuvant therapy in colon cancer: observations based on individual patient data from 20,898 patients on 18 randomised trials.* J. Clin. Oncol., 27 (2009), 872–877.

[55] E.D. Schwab, K.J. Pienta. *Cancer as a complex adaptive system.* Medical Hypotheses, 47 (1996), 235–241.

[56] J.A. Spratt, D. von Fournier, J.S. Spratt, E.E. Weber. *Decelerating growth and human breast cancer.* Cancer, 71 (1993), no. 6, 2013–2019.

[57] M.Z. Tesfay, A.C. Kirk, E.M. Hadac, G.E. Griesmann, M.J. Federspiel G.N. Barber, S.M. Henry, K.W. Peng, S.J. Russell. *PEGylation of vesicular stomatitis virus extends virus persistence in blood circulation of passively immunized mice.* J. Virol, 87 (2013), no. 7, 3752–3759.

[58] L.M. Wein, J.T. Wu, D.H. Kirn. *Validation and analysis of a mathematical model of a replication-competent oncolytic virus for cancer treatment: implications for virus design and delivery.* Cancer Res., 63 (2003), 1317–1324.

[59] K.P. Wilkie, P. Hahnfeldt. *Modelling the dichotomy of the immune response to cancer: cytotoxic effects and tumor-promoting inflammation.* ArXiv, 1305.3634 (2014), 1–24.

[60] M.A. Williams, M.J. Bevan. *Effector and memory CTL differentiation.* Annu. Rev. Immunol., 25 (2007), 171–192.

[61] D. Wodarz. *Viruses as antitumor weapons: defining conditions for tumor remission.* Cancer Res., 61 (2001), 3501–3507.

[62] D. Wodarz. *Computational modelling approaches to studying the dynamics of oncolytic viruses.* Mathematical Biosciences and Engineering, 10 (2013), 939–957.

[63] D. Wodarz, A. Hofacre, J.W. Lau, Z. Sun, H. Fan, N.L. Komarova. *Complex spatial dynamics of oncolytic viruses in vitro: mathematical and experimental approaches.* PLoS Comput. Biol., 8 (2011), no. 6, e1002547.

[64] D. Wodarz, N. Komarova. *Towards predictive computational models of oncolytic virus therapy: basis for experimental validation and model selection.* PLoS One, 4 (2009), no. 1, e4271.

[65] A. Wolf, J.B. Swift, H.L. Swinney, J.A. Vastano. *Determining Lyapunov exponents from a time series.* Physica D, 16 (1985), 285–317.

[66] J.T. Wu, H.M. Byrne, D.H. Kirn, L.M. Wein. *Modelling and analysis of a virus that replicates selectively in tumor cells.* Bull. Math. Biol., 63 (2001), no. 4, 731–768.

Raluca Eftimie, Cicely K. Macnamara, Jonathan Dushoff, Jonathan L. Bramson, David J.D. Earn
Bifurcation and Chaos in Tumour Dynamics

[67] A. Zippelius, P. Batard, V. Rubio-Godoy, G. Bioley, D. Liénard, F. Lejeune, D. Rimoldi, P. Guillaume, N. Meidenbauer, A. Mackensen, N. Rufer, N. Lubenow, D. Speiser, J.-C. Cerottini, P. Romero, M.J. Pittet. *Effector function of human tumour-specific CD8 T cells in melanoma lesions: a state of local functional tolerance.* Cancer Res., 64 (2004), 2865–2873.